Phase-locking of laminar wake to periodic vibrations of a circular cylinder

M. A. Khodkar ●,[1,*] Joseph T. Klamo ●,[2,†] and Kunihiko Taira ●[1,‡]

[1]*Department of Mechanical and Aerospace Engineering, University of California,*
Los Angeles, California 90095, USA
[2]*Department of Systems Engineering, Naval Postgraduate School,*
Monterey, California 93943, USA

Phase synchronization between the vortex shedding behind a two-dimensional circular cylinder and its vibrations is investigated using the phase-reduction analysis. Leveraging this approach enables the development of a one-dimensional, linear model with respect to the limit-cycle attractor of the laminar wake, which accurately describes the phase dynamics of the high-dimensional, nonlinear fluid flow and its response to rotational, transverse, and longitudinal vibrations of the cylinder. This phase-based model is derived by assessing the phase response and sensitivity of the wake dynamics to impulse perturbations of the cylinder, which can be performed in simulations and experiments. The resulting model in turn yields the theoretical conditions required for phase-locking between the cylinder vibrations and the wake. We furthermore show that this synchronization mechanism can be employed to stabilize the wake and subsequently reduce drag. We also uncover the circumstances under which the concurrent occurrence of different vibrational motions can be used to promote or impede synchronization. These findings provide valuable insights for the study of vortex-induced body oscillations, the enhancement of aerodynamic performance of flyers, and the mitigation of structural vibrations by synchronizing or desynchronizing the oscillatory motions of a body to the periodic wake.

I. INTRODUCTION

Understanding the dynamics of the wake behind a bluff body immersed in a moving fluid is critical for predicting the fluctuating pressure field and the resulting forces on the body. By manipulating the wake directly behind an object, one can decrease drag on a body, increase lift on a foil, or improve energy harvesting of the system. Moreover, the characteristics of the downstream wake can influence mixing performance and increase the reaction rate of combustion processes.

The oscillating wake behind a cylinder in a moving fluid was first studied by Strouhal in 1878 [1]. However, it was not until the late 1960s that researchers investigated the effects of an actively moving cylinder on the synchronization of shed vortices in the wake. These studies pulsed a piezoelectric material positioned between two hemispheres [2], forced a circular cylinder to move transverse to the flow [3], and allowed a circular cylinder to freely vibrate normal to the flow [4]. Each of these different excitation methods caused the vortex shedding frequency to synchronize

---

*mkhodkar@ucla.edu

†jklamo@nps.edu

‡ktaira@seas.ucla.edu

with the frequency of the cylinder motion when the frequency of that motion was close to the natural shedding frequency of the flow. These investigations confirmed that the controlled excitation of a cylinder at frequencies close to the vortex shedding frequency for a stationary cylinder resulted in important changes to the wake. An enormous amount of research has since been carried out exploring various aspects of forced and free vibrations of cylinders in a free stream. These results are described in the numerous review articles [5–11] on forced and free vibration of cylinders. An important finding from these investigations was the synchronization of the wake shedding frequency to the oscillating frequency of the cylinder. The term "lock-in" was coined to describe such behavior.

Subsequent research has enhanced our understanding of synchronization and led to important insights. A flow visualization study [12] identified the various wake structures behind an oscillating cylinder and the approximate location of the synchronization boundaries for Re = 1000. Perhaps the most important finding of their work was the observation that the wake can change significantly at frequencies not necessarily "close" to the natural shedding frequency. This study revealed the existence of a much larger synchronization region than initially understood. Moreover, the study reported the observation of two different wake structures within the synchronization region. In an ensuing study, a dense parametric sweep of the amplitude and frequency space of a forced oscillating cylinder was completed to precisely identify the synchronization boundaries and two wake structures at Re = 4000 and 12 000 [13].

The importance of the vortex-induced vibration (VIV) of structures for a range of engineering problems has been identified in the past few decades. The practical applications of VIV can be commonly seen in offshore platforms, heat exchangers, transmission lines, and marine cables [9–11,14]. Identification and prediction of the synchronization region are the critical aspect of VIV. The reason is because the free vibration of a structure specifically occurs when the wake is inside the synchronization region.

Despite 50 years of research involving forced and free cylinder vibrations, there has been no technique to predict the boundaries of the synchronization region in the frequency-amplitude plane. Instead, we must laboriously find it experimentally or numerically through an extensive parametric study for a particular Reynolds number and cylinder shape of interest. To address this shortcoming, we put forth a phase-based analysis capable of identifying the synchronization region. This approach requires only a limited set of experimental or numerical results to identify the phase sensitivity to various perturbations. The approach was previously used on the phase response to external excitation of low-Reynolds-number laminar wakes [15,16]. In our study, we apply the phase-reduction analysis to flows in which the body is forced to oscillate in a rotary, cross-flow (transverse), or streamwise (in-line) fashion. We develop a linear, one-dimensional model with respect to the limit cycle (periodic flow) that accurately characterizes the conditions necessary for synchronization between the vortex shedding frequency and the periodic cylinder vibrations. This model can further be utilized to examine how the concurrent presence of different vibrational modes, e.g., simultaneous rotary and cross-flow vibrations, might allow for widening or narrowing the synchronization region.

The organization of the paper is as follows. The phase-based model is developed in Sec. II. Section III A begins with a short description of the numerical solver used for conducting the direct numerical simulations (DNSs) of the flow. We further present the phase properties of the flow for various types of cylinder oscillations, obtained by introducing impulsive perturbations of the cylinder at several times over a period in the DNS code. Section III B renders the model predictions for synchronization regions and shows their accuracy by comparing them to the present DNS results as well as earlier experimental and numerical data. It also discusses the effect of phase-locking between the vortex shedding and cylinder oscillation on the wake structure and, consequently, lift and drag. Section III C demonstrates how the synchronization region of the periodic flow can be altered by superimposing different vibrational motions. Section IV concludes the paper with a summary of principal findings and their practical implications.

II. PHASE REDUCTION OF PERIODIC FLOWS

Let us consider the dynamics of an incompressible flow described by

$$\dot{\boldsymbol{q}} = \boldsymbol{N}(\boldsymbol{q}), \tag{1}$$

where $\boldsymbol{q}$ is the state vector of the flow. In this paper, we focus on the dynamics with respect to a stable limit cycle $\boldsymbol{q_0}$, for which the flow is periodic, satisfying $\boldsymbol{q_0}(\boldsymbol{x}, t + T) = \boldsymbol{q_0}(\boldsymbol{x}, t)$. Here, T denotes the periodicity, which is related to the natural frequency ω_n by $\omega_n = 2\pi/T$. Due to the periodic nature of this base flow, its phase dynamics can be represented by

$$\dot{\theta} = \omega_n, \quad \theta \in [-\pi, \pi], \tag{2}$$

where θ is the phase of the limit-cycle oscillation. When the state does not reside on the limit-cycle attractor, but instead lies in its basin, the phase dynamics can be characterized by the phase function $\Theta(\boldsymbol{q})$ such that $\theta = \Theta(\boldsymbol{q})$. The use of $\Theta(\boldsymbol{q})$ in Eq. (2) yields

$$\dot{\theta} = \dot{\Theta}(\boldsymbol{q}) = \nabla_{\boldsymbol{q}} \Theta(\boldsymbol{q}) \cdot \dot{\boldsymbol{q}} = \nabla_{\boldsymbol{q}} \Theta(\boldsymbol{q}) \cdot \boldsymbol{N}(\boldsymbol{q}) = \omega_n. \tag{3}$$

Here, the phase function $\Theta(\boldsymbol{q})$ extends the definition of phase in the vicinity of the limit cycle.

Now, consider the introduction of a weak perturbation to the fluid system of Eq. (1),

$$\dot{\boldsymbol{q}} = \boldsymbol{N}(\boldsymbol{q}) + \epsilon \boldsymbol{f}(t), \tag{4}$$

with $\epsilon \ll 1$ and $\|\boldsymbol{f}\|_2 = 1$. This equation can be rewritten in terms of the phase function to obtain

$$\dot{\theta} = \dot{\Theta}(\boldsymbol{q}) = \nabla_{\boldsymbol{q}} \Theta(\boldsymbol{q}) \cdot \dot{\boldsymbol{q}} = \nabla_{\boldsymbol{q}} \Theta(\boldsymbol{q}) \cdot [\boldsymbol{N}(\boldsymbol{q}) + \epsilon \boldsymbol{f}(t)], \tag{5}$$

which along with Eq. (3) gives

$$\dot{\theta} = \omega_n + \epsilon \nabla_{\boldsymbol{q}} \Theta(\boldsymbol{q})|_{\boldsymbol{q}=\boldsymbol{q_0}} \cdot \boldsymbol{f}(t), \tag{6}$$

where we have neglected the higher-order terms and derived a linear model with respect to the limit cycle $\boldsymbol{q_0}(t)$. This equation describes the phase dynamics of the nonlinear and high-dimensional flow only via a scalar phase variable. In the rest of the paper, $\nabla_{\boldsymbol{q}} \Theta(\boldsymbol{q})|_{\boldsymbol{q}=\boldsymbol{q_0}}$ is denoted by $\boldsymbol{Z}(\theta)$ and is called the phase-sensitivity function.

The focus of the present work is to develop a general framework which can be implemented both numerically and experimentally. Therefore, adjoint-based approaches requiring the explicit knowledge of governing equations [17,18] are not pursued, and instead, a direct method, which evaluates $\boldsymbol{Z}$ by applying weak impulse perturbations at different times (phases) over a period, is employed. These impulses are in the form $I\delta(t - t_0)\hat{\boldsymbol{e}}_j$, where I, $\delta(t - t_0)$, and $\hat{\boldsymbol{e}}_j$ respectively indicate the perturbation amplitude, a Dirac delta function centered at t_0, and the unit vector in the direction of the impulse. The delta function $\delta(t - t_0)$ is modeled as the following narrow Gaussian function in the numerical solver:

$$\delta(t - t_0) = \frac{1}{\sqrt{2\pi}\sigma} \exp\left[-\frac{1}{2}\left(\frac{t - t_0}{\sigma}\right)^2\right], \tag{7}$$

where $\sigma = 10\Delta t$, with Δt being the DNS time step (Sec. III A).

After a sufficiently long time, the transient effects of adding impulse perturbation to the periodic flow vanish, and the state of the flow relaxes to its limit cycle. However, the impulse creates an asymptotic phase shift, referred to as the phase-response function $g(\theta; I\hat{\boldsymbol{e}}_j)$, which can be measured for any given phase θ at which the flow is initially perturbed. The phase-sensitivity function $\boldsymbol{Z}$ is then calculated as

$$Z_j(\theta) = \lim_{I \to 0} \frac{g(\theta; I\hat{\boldsymbol{e}}_j)}{I} \approx \frac{g(\theta; I\hat{\boldsymbol{e}}_j)}{I}, \tag{8}$$

assuming that $I \ll 1$. Repeating the same procedure for different values of θ over the entire period provides the 2π-periodic phase-sensitivity function [15,18].

Synchronization or phase-locking between the periodic flow and any harmonic oscillators (e.g., external actuations and forced or flow-induced body vibrations) can be achieved if and only if the temporal change $\dot{\phi}$ in the phase difference between the flow and the forced oscillator [$\phi = \theta(t) - \omega_f t$] approaches zero, while the oscillator's frequency ω_f is not very different from ω_n or its harmonics. Substituting $\dot{\theta}$ from Eq. (6) enables expressing this synchronization condition in the following analytical form:

$$\dot{\phi} = \epsilon[\Delta + \mathbf{Z}(\phi + \omega_f t) \cdot \boldsymbol{f}(t)] \to 0, \tag{9}$$

where $\Delta = (\omega_n - \omega_f)/\epsilon = O(1)$.

Since $\dot{\phi} \ll \omega_f$, the right-hand side of Eq. (9) can be approximated by its mean over one period [17,19], leading to

$$\dot{\phi} = \epsilon[\Delta + \Gamma(\phi)], \tag{10}$$

where the 2π-periodic phase-coupling function $\Gamma(\phi)$ is formulated as

$$\Gamma_m(\phi) = \frac{\omega_f}{2\pi} \int_{-\pi/\omega_f}^{\pi/\omega_f} \mathbf{Z}(\phi + \omega_f \tau/m) \cdot \boldsymbol{f}(\tau)d\tau = \frac{1}{2\pi} \int_{-\pi}^{\pi} \mathbf{Z}(\phi + \varphi/m) \cdot \boldsymbol{f}(\varphi)d\varphi, \tag{11}$$

with $m \in \mathbb{N}$ indicating the number of the harmonic at which the synchronization is investigated. For the mth harmonic, synchronization to the frequency $m\omega_n$ can be studied. Stable phase-locking between the oscillator and the periodic flow requires

$$\epsilon\Gamma_{\min} < \omega_f/m - \omega_n < \epsilon\Gamma_{\max}, \tag{12}$$

where the minimum and maximum values of Γ are denoted by $\Gamma_{\max}$ and $\Gamma_{\min}$, respectively. Note that, in this study, phase-locking at higher harmonics ($m > 1$) is always subharmonic, as will be discussed in Sec. III. In a subharmonic synchronization, the periodic flow is synchronized to ω_f/m instead of ω_f. Equation (12) suggests that the region of synchronization in the frequency-amplitude plane, also known as the Arnold tongue [20], grows with $\Gamma_{\max} - \Gamma_{\min}$. The synchronizability parameter $S \equiv \Gamma_{\max} - \Gamma_{\min}$ is thus defined as a measure to quantify how easily phase-locking can occur.

III. PHASE SYNCHRONIZATION OF WAKE FLOW TO CYLINDER OSCILLATIONS

We explore the influence of fundamental vibrational motions of the cylinder on the synchronization properties of the wake flow. This section commences with a brief description of the DNS solver used for simulating the two-dimensional (2D) incompressible flow over the oscillating cylinder. It further presents the phase-sensitivity and phase-coupling functions obtained using perturbed DNS simulations. In the latter part of the section, the theoretical and numerical Arnold tongues are compared, and the possibility of stabilizing the wake via cylinder vibrations is investigated. The section is concluded by discussing the impact of combining different types of oscillations on the synchronizability of the periodic wake.

A. Numerical solver

The dimensionless governing equations of a 2D incompressible flow are

$$\frac{\partial \boldsymbol{u}}{\partial t} + \boldsymbol{u} \cdot \nabla \boldsymbol{u} = -\nabla p + \frac{1}{\text{Re}}\nabla^2 \boldsymbol{u}, \quad \nabla \cdot \boldsymbol{u} = 0. \tag{13}$$

Here, $\boldsymbol{u}$ and p represent the nondimensional velocity and pressure fields, respectively, while the cylinder diameter d and the free-stream velocity U are selected as the characteristic length and velocity (Fig. 1). The Reynolds number is defined as $\text{Re} \equiv Ud/\nu$, where ν is the kinematic viscosity. In all considered cases, we set $\text{Re} = 100$. The lift coefficient C_L and its time derivative $\dot{C}_L$ are used to determine the phase with $\theta = \tan^{-1}(C_L/\dot{C}_L)$.
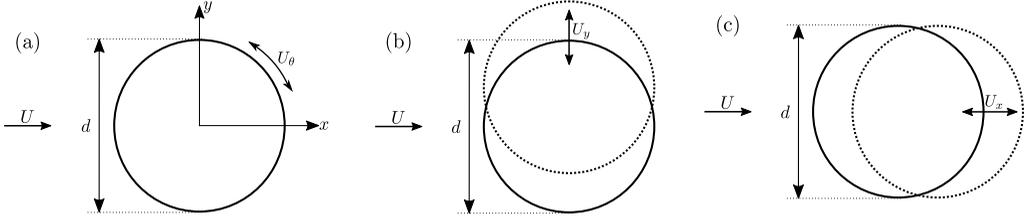
FIG. 1. Schematic of a uniform flow past a 2D circular cylinder, when the cylinder oscillates in a (a) rotary, (b) streamwise, or (c) cross-flow fashion, with the respective tangential, streamwise, or cross-flow velocities U_θ, U_x, and U_y. All these velocities are given by $U_f \sin(\omega_f t)$, with U_f and ω_f indicating the velocity oscillation amplitude and frequency, respectively.

The immersed boundary projection method [21] is utilized to conduct the DNS of the flow, with the multidomain technique [22] employed for far-field boundary conditions. The center of the cylinder is located at the origin, and the computational domain is stretched over $(x/d, y/d) \in [-39.5, 40.5] \times [-40, 40]$. The horizontal and vertical spacings of the finest domain, which is the one closest to the cylinder, are uniform, with $\Delta x/d = \Delta y/d = 0.025$. The time step $\Delta t = 0.005$ satisfies $U \Delta t/\Delta x < 0.5$. The natural shedding frequency ω_n, the aerodynamic forces on the cylinder, and the velocity and vorticity fields provided by the unperturbed computational setup of this section agree closely with those of previous works [15,23].

To determine the phase-sensitivity function of rotary oscillation, the cylinder is impulsively moved with the tangential velocity $U_\theta = U_f \delta(t - t_0)$ [Fig. 1(a)] at different phases over a period. For the cross-flow and streamwise oscillations, body oscillations are incorporated in the reference frame of the body by subtracting the cylinder speed $U_x = U_f \delta(t - t_0)$ or $U_y = U_f \delta(t - t_0)$ from the free-stream velocity [Figs. 1(b) and 1(c)]. These impulses are introduced to the governing equations as accelerations to the reference frame of the body and are numerically enforced by modifying the boundary conditions. The phase-sensitivity function associated with each case is then calculated by determining the asymptotic phase shift in the time series of C_L and is depicted in Fig. 2(a). Lift and drag are evaluated in the reference frame moving with the cylinder. We also remark that the linearity assumption of Sec. II necessitates choosing $U_f \leqslant 0.05$ ($U_f \leqslant 0.025$) for rotary and cross-flow oscillations (streamwise oscillation).
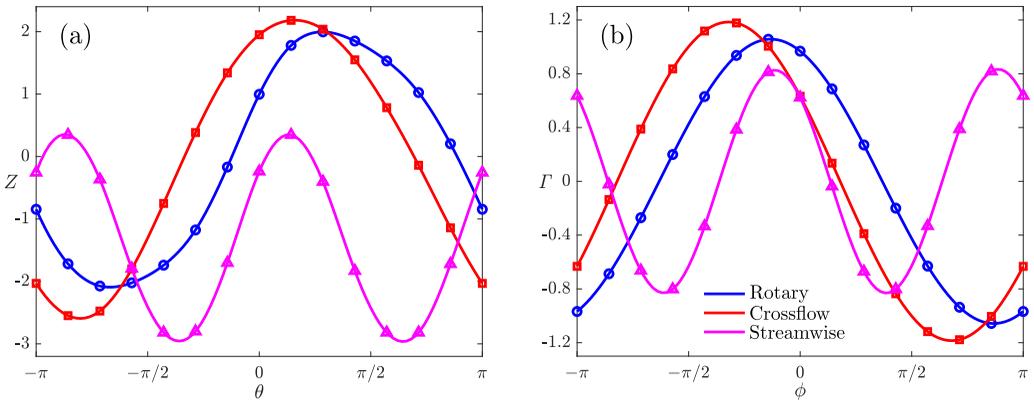
FIG. 2. (a) Phase sensitivity Z and (b) phase-coupling functions Γ for different types of cylinder oscillations. Note that presented Γ for the rotary and cross-flow oscillations are the first-harmonic phase-coupling functions, while that of the streamwise oscillation is calculated at the second harmonic.
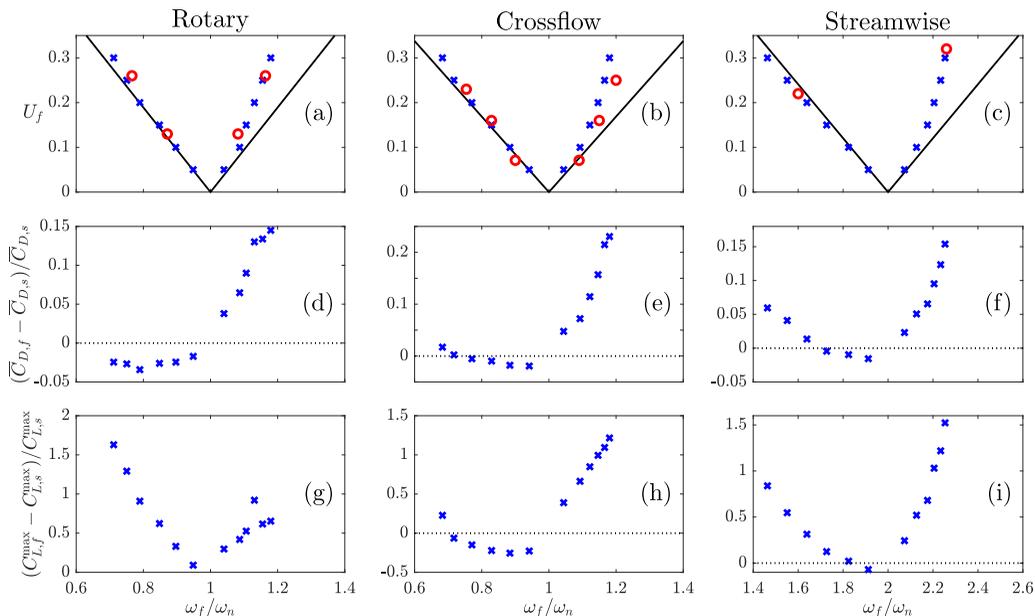
FIG. 3. Top: Theoretical and numerical boundaries of synchronization for (a) rotary, (b) cross-flow, and (c) streamwise oscillations in the frequency-amplitude plane, indicated by black solid lines and blue crosses, respectively. Middle: Time-averaged drag coefficients $\overline{C}_D$ for the synchronized cases of (d) rotary, (e) cross-flow, and (f) streamwise oscillations. Bottom: Same as the middle, but for maximum lifts $C_L^{\max}$. Subscripts f and s refer to the oscillatory and stationary cylinder cases, respectively. Horizontal dotted lines represent zero values, or when the cylinder is at rest. Red circles in (a)–(c) show the numerical results of [28] at Re = 110, the experimental observations of [3] at Re = 100, and the findings of [26] at Re = 80, respectively.

Once the phase-sensitivity function Z is found, the corresponding phase-coupling function Γ is obtained from Eq. (11) and is displayed in Fig. 2(b). Although the phase-sensitivity functions of rotary and cross-flow oscillations peak at different phase values, their maximum and minimum values are fairly close. In addition, both oscillations yield similar values for the synchronizability at the first harmonic ($S = 2.11$ and 2.37, respectively, for the rotary and cross-flow oscillations) and very small values for the synchronizability at the second harmonic [$S = O(0.01)$ for both], confirming the observations of former studies that rotary and transverse vibrations exhibit only first-harmonic synchronization [24,25]. The π periodicity of the phase-sensitivity function for the steamwise oscillation is also consistent with the findings of earlier investigations [26,27], demonstrating that the wake flow synchronizes to the in-line oscillation only subharmonically at the second harmonic, as this property results in $S \approx 0$ at the first harmonic and much larger values for synchronizability ($S = 1.66$) at the second harmonic.

B. Synchronization and force properties

The Arnold tongues (solid lines) revealed by the phase-reduction analysis for rotary, cross-flow and streamwise oscillations are compared to the corresponding boundaries of synchronization obtained from DNS (blue crosses) in Fig. 3, for which U_θ, U_x, or U_y is given by $U_f \sin(\omega_f t)$. While synchronization to the natural shedding frequency is considered for the rotary and cross-flow vibrations, the synchronization of the streamwise oscillation is studied at its second harmonic. The blue crosses correspond to the oscillation frequencies that maximize $|\omega_f - m\omega_n|$ for a specified value of U_f while maintaining the difference between the shedding frequency and ω_f below 1%. The red circles are the results extracted from previous studies [3,26,28], with Re varying from 80

to 110. The left branches of the present numerical and theoretical boundaries of synchronization are in good agreement up to large values of velocity oscillation amplitude ($U_f \lesssim 0.25$). In contrast, on the right branch of the Arnold tongues, agreement is limited to moderate oscillation amplitudes ($U_f \lesssim 0.1$).

As U_f gradually increases, the state of the flow departs farther from its stable limit cycle, and as a result, nonlinear effects become progressively more manifest. We should also notice that however the phase-reduction theory yields $|\Gamma_{\max}| = |\Gamma_{\min}|$ when the oscillatory motion of the cylinder is governed by a zero-mean periodic function, thus predicting identical slopes for the left and right branches of the Arnold tongues, in actual systems, this symmetry does not hold, particularly at large oscillation amplitudes. Accelerating the vortex shedding process leads to a narrower vortex formation region. Due to the physical constraint imposed on the length of the vortex formation region, it is taxing to diminish this parameter beyond a certain point and, as a result, to synchronize the wake to frequencies much higher than ω_n [29,30]. Consequently, in accordance with the findings of earlier investigations, delaying the vortex shedding process by phase-locking it to oscillation frequencies below ω_n uses less actuation amplitudes than when the shedding is advanced, assuming that the desired frequency shift is identical for both, as the latter requires larger oscillation amplitudes [3,28,31]. This is of aerodynamic importance since delaying vortex shedding is the primary mechanism for reducing the wake unsteadiness and, subsequently, lowering drag at the Reynolds number and frequencies under consideration, whereas accelerating the shedding process affects the aerodynamic performance by exciting the shear-layer instability only at higher Reynolds numbers (Re $\gtrsim 500$) and frequencies ($\omega_f \gtrsim 4\omega_n$) [32]. It is thus encouraging to find that the aerodynamically advantageous strategy needs a smaller amplitude for control inputs and can be accurately predicted using the present phase-based model. Among all three oscillatory modes studied in the current work, the rotary oscillation leads to the largest drag reduction, by around 4% with respect to the stationary cylinder case [Figs. 3(d)–3(f)]. The difference between the time-averaged vorticity fields of the synchronized wake flows of Fig. 3 minimizing $\overline{C}_D$ and that of the base flow (stationary cylinder case) is portrayed in Fig. 4 for all three oscillatory motions. As shown in Fig. 4, a lower value for $\overline{C}_D$ corresponds to a more elongated and streamlined wake caused by delayed vortex shedding. For each panel of Fig. 4, a video demonstrating the evolution of the corresponding vorticity field is included in the Supplemental Material [33]. Maximum lift coefficients $C_L^{\max}$ can also be altered by cylinder vibration, as shown in Figs. 3(g)–3(i). Cross-flow oscillation noticeably reduces the amplitudes of lift when the vortex shedding is phase-locked to $0.75 \lesssim \omega_f/\omega_n \lesssim 1$. The synchronized cases on the right branch of the Arnold tongues augment $C_L^{\max}$, with cross-flow and streamwise oscillations being more effective.

C. Concurrent vibrations

In real-world examples, structural vibrations or oscillatory motions of flyers are typically a combination of the aforementioned vibrational modes [9,11]. It is thus practically more important to analyze scenarios in which all these motions occur simultaneously. Combining the streamwise oscillation with any of the other motions breaks the π periodicity of the phase-sensitivity function and the symmetry of the in-line oscillation with respect to the centerline of the wake flow, leading to no lock-on to the second harmonic. Furthermore, since the phase-coupling function of the streamwise oscillation is nearly vanishing at the first harmonic, the synchronization properties of the flow at the this harmonic are negligibly affected by the presence of this oscillation. Hence, we confine our attention to the superposition of rotary and cross-flow oscillations in what follows.

Suppose that the cylinder oscillates rotationally and transversely at the same frequency, but with different amplitudes and phases. The combined motion can be mathematically expressed as

$$\boldsymbol{f}(t) = 2U_f[\alpha \sin(\omega_f t + \phi_f)\hat{\boldsymbol{e}}_{\boldsymbol{\theta}} + (1 - \alpha)\sin(\omega_f t)\hat{\boldsymbol{e}}_{\boldsymbol{y}}], \qquad (14)$$

where ϕ_f is the phase difference between the rotary and cross-flow vibrations and the weight α varies from 0 to 1. The unit vectors $\hat{\boldsymbol{e}}_{\boldsymbol{\theta}}$ and $\hat{\boldsymbol{e}}_{\boldsymbol{y}}$ are oriented in the tangential and vertical directions,
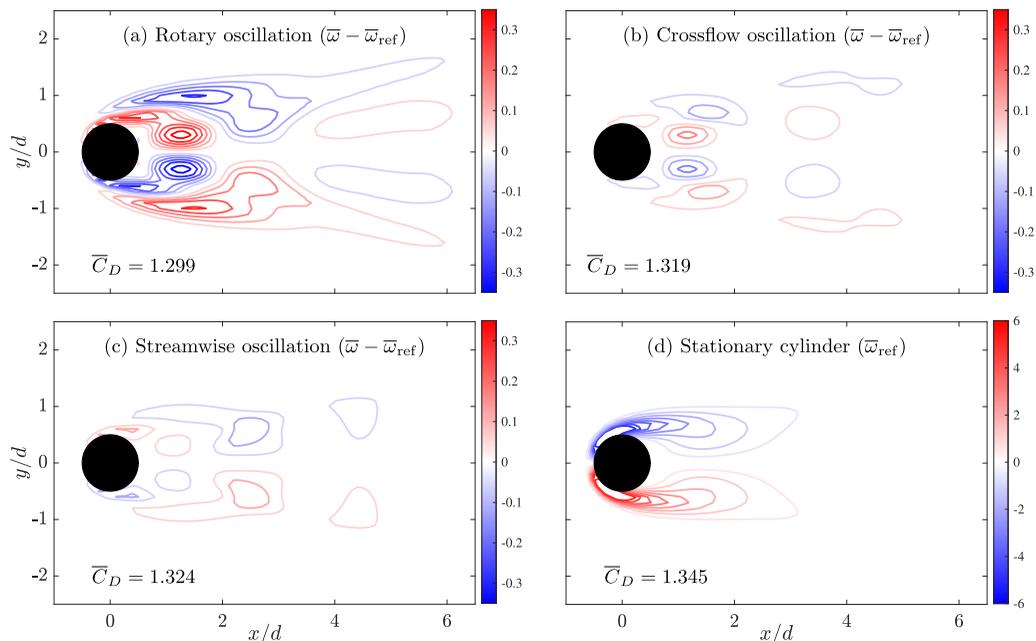
FIG. 4. (a)–(c) The time-averaged vorticity fields of the synchronized cases with the lowest mean drag coefficient $\overline{C}_D$ ($\overline{\omega}$), substracted from that of the stationary cylinder $\overline{\omega}_{\text{ref}}$ shown in (d) to illustrate the wake elongations for the three cases. (d) Time-averaged vorticity field of the base flow.

respectively. The synchronizability of the motion described by Eq. (14) is demonstrated as functions of α and ϕ_f in Fig. 5. The synchronizability is maximized when the cylinder motion is a purely cross-flow vibration ($\alpha = 0$). The results of this case were studied in detail in Sec. III B. The blue circle in Fig. 5(a) with $\alpha = 0.53$ and $\phi_f = 0.82\pi$ corresponds to the point at which synchronizability is the lowest ($S = 0.064$). The green circle represents the case at which the rotary and cross-flow oscillations are added with the same amplitude and no phase difference ($\alpha = 0.5$ and $\phi_f = 0$). As expected, rotary and cross-flow oscillations occurring simultaneously with the same amplitude and
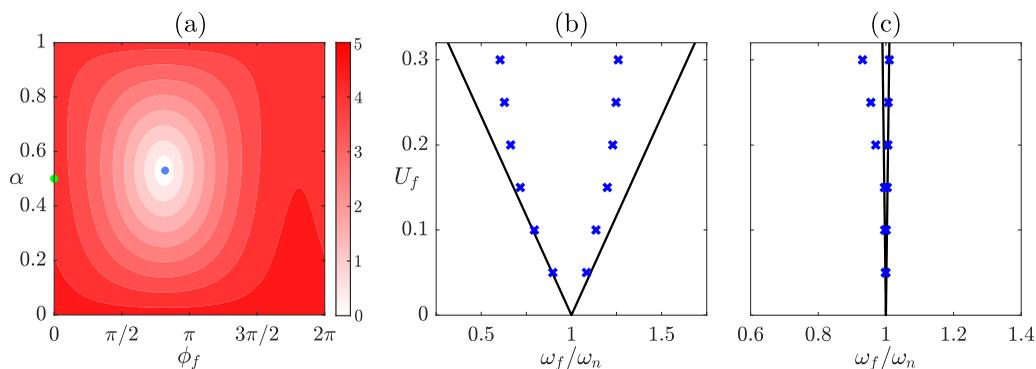
FIG. 5. (a) Synchronizability as a function of the weight α and phase difference ϕ_f of concurrent rotary and cross-flow oscillations. (b) Theoretical (solid lines) and numerical (blue crosses) Arnold tongues corresponding to the green point in (a) for which $\alpha = 0.5$ and $\phi_f = 0$. (c) Same as (b), but for the blue point in (a) at which synchronizability is minimized.

phase amplify each other's synchronization properties, as the phase-sensitivity functions of the two oscillations are nearly in phase [Fig. 2(a)]. Consequently, the resulting Arnold tongue [Fig. 5(b)] is almost twice as wide as the Arnold tongues for flows in which only one of the vibrational modes is present [Figs. 3(a) and 3(b)]. This enables synchronization with frequencies much farther from ω_n for a fixed value of U_f. On the other hand, the proper choice for the amplitude and phase difference of the two oscillations can result in $S \approx 0$, as can be seen in Fig. 5(c). However, the numerical synchronization region is slightly wider than that predicted by the phase-based model (especially at large amplitudes); overall, the present model proves successful in proposing strategies for combining various vibrational motions that lead to the amplification or attenuation of the synchronization properties of the wake flow.

In a more comprehensive case, the two vibrations might not have the same frequency, which can give rise to a quasiperiodic flow with two dominant frequencies if the cylinder wake synchronizes to both oscillations. Such a case is beyond the scope of the present work, as it cannot be characterized by a single limit-cycle attractor, and therefore is not studied here.

In addition to enabling the analysis of realistic flows that incorporate complex structural vibrations or body oscillations, the present framework shows promise for designing optimal control strategies for achieving a desired aerodynamic target, e.g., an increased lift or a reduced drag, with the methodical superposition of different vibrational modes or the introduction of external oscillators such as periodic actuations to the wake flow of a vibrating body. Furthermore, the resonance between the periodic flow and vortex-induced body vibrations can be prevented by substantially shrinking the synchronization region of the flow, as performed for the example studied in this section, averting structural damages. As noted by Bearman [7], flows past a forcibly oscillating body and a freely vibrating one are assumed to produce nearly identical patterns as long as the amplitude and frequency of oscillations as well as the Reynolds number of the flows are the same. We thus reasonably expect that the general conclusions of this study hold for dynamics related to vortex-induced vibrations.

IV. CONCLUDING REMARKS

A detailed phase-based analysis of the response of a 2D periodic cylinder wake to excitations due to the cylinder vibrations was conducted. This analysis provided a theoretical approach for prediction of the required excitation amplitude and frequency to cause synchronization of the wake to the cylinder motion. The criteria for wake synchronization to rotary, cross-flow, and streamwise vibrations of the cylinder at Re = 100 were determined. A direct method was utilized which relies on impulsively perturbing the cylinder (or free-stream velocity) at different times during the shedding cycle to reveal the phase response and sensitivity of the wake dynamics to the cylinder vibrations. This method avoids dealing with equations that capture the complex dynamics of the wake, and its numerical or experimental execution is straightforward and inexpensive. Our theoretical predictions for the synchronization region at Re = 100 for all three vibrational motions showed good agreement with a limited set of previous experimental data and a larger set of data generated by the present study. Finally, we demonstrated the possibility of widening or narrowing the synchronization region by combining the fundamental modes of vibration.

Although the authors anticipate that the general findings of the present work remain valid for practical applications of VIV that occur at higher Reynolds numbers, further work is needed for confirmation. We plan to examine the accuracy of the predicted synchronization boundaries using our phase-reduction analysis for each fundamental vibrational mode to experimentally determined ones at higher Re = $O(10^3)$. This would confirm whether the linear phase-based approach is sufficient to handle the complex and fully three-dimensional wakes emerging in actual VIV scenarios. If portions of the predicted synchronization boundaries at higher Reynolds numbers are not predicted accurately enough, such as the higher-frequency side branch, then the inclusion of higher-order terms in the analysis is possible. These higher Reynolds numbers will also ensure that both the 2S and 2P wake structures, observed in previous studies [12,13,34], exist in different

sections of the synchronization. This will allow us to demonstrate that not only can we identify the synchronization region boundaries, but also the boundary between these two wake structures within the synchronization region can be detected using this phase-based methodology.

The phase-based model has remarkable potential once the accuracy of the approach at predicting the conditions leading to phase-locking between the vortex shedding and cylinder vibrations at higher Reynolds number can be established. A whole new direction of VIV research can be guided by our finding that the coupling of two different vibrational modes can either widen or narrow the synchronization region. A wider region allows for synchronization to be achieved using lower amplitudes which require less excitation. On the other hand, narrowing the region would provide another approach, other than using strakes, to suppress VIV. This can be attained through small, multiple-degree-of-freedom motions to keep the wake unsynchronized and thereby substantially mitigate structural fatigue.

ACKNOWLEDGMENTS

[1] V. Strouhal, Ueber eine besondere art der tonerregung, Ann. Phys. (Berlin, Ger.) **241**, 216 (1878).

[2] O. H. Wehrmann, Reduction of velocity fluctuations in a Kàrmàn vortex street by a vibrating cylinder, Phys. Fluids **8**, 760 (1965).

[3] G. H. Koopmann, The vortex wakes of vibrating cylinders at low Reynolds numbers, J. Fluid Mech. **28**, 501 (1967).

[4] N. Ferguson, The measurement of wake and surface effects in the subcritical flow past a circular cylinder at rest and in vortex-excited oscillation, MS thesis, University of British Columbia, 1965.

[5] T. Sarpkaya, Vortex-induced oscillations: A selective review, J. Appl. Mech. **46**, 241 (1979).

[6] O. M. Griffin and S. E. Ramberg, Some recent studies of vortex shedding with application to marine tubulars and risers, J. Energy Res. Technol. **104**, 2 (1982).

[7] P. W. Bearman, Vortex shedding from oscillating bluff bodies, Ann. Rev. Fluid Mech. **16**, 195 (1984).

[8] G. Parkinson, Phenomena and modelling of flow-induced vibrations of bluff bodies, Prog. Aerospace Sci. **26**, 169 (1989).

[9] E. Naudascher and D. Rockwell, *Flow-Induced Vibrations: An Engineering Guide* (Balkema, Rotterdam, 1994).

[10] T. Sarpkaya, A critical review of intrinsic nature of vortex-induced vibrations, J. Fluids Struct. **19**, 389 (2004).

[11] C. H. K. Williamson and R. Govardhan, Vortex-induced vibrations, Annu. Rev. Fluid Mech. **36**, 413 (2004).

[12] C. H. K. Williamson and A. Roshko, Vortex formation in the wake of an oscillating cylinder, J. Fluids Struct. **2**, 355 (1988).

[13] T. L. Morse and C. H. K. Williamson, Prediction of vortex-induced vibration response by employing controlled motion, J. Fluid Mech. **634**, 5 (2009).

[14] R. King, A review of vortex shedding research and its application, Ocean Engineering **4**, 141 (1977).

[15] K. Taira and H. Nakao, Phase-response synchronization for analysis of periodic flows, J. Fluid Mech. **846**, R2 (2018).

[16] M. A. Khodkar and K. Taira, Phase-synchronization properties of laminar cylinder wake for periodic external forcings, J. Fluid Mech. **904**, R1 (2020).

[17] G. B. Ermentrout and D. H. Terman, *Mathematical Foundations of Neurosience* (Springer, New York, 2010).

[18] H. Nakao, Phase reduction approach to synchronisation of nonlinear oscillators, Contemp. Phys. **57**, 188 (2016).

[19] Y. Kuramoto, *Chemical Oscillations, Waves, and Turbulence* (Springer, Berlin, 1984).

[20] V. I. Arnold, *Mathematical Methods of Classical Mechanics* (Springer, New York, 1997).

[21] K. Taira and T. Colonius, The immersed boundary method: A projection approach, J. Comput. Phys. **225**, 2118 (2007).

[22] T. Colonius and K. Taira, A fast immersed boundary method using a nullspace approach and multi-domain far-field boundary conditions, Comput. Methods Appl. Mech. Eng. **197**, 2131 (2008).

[23] P. M. Munday and K. Taira, On the lock-on of vortex shedding to oscillatory actuation around a circular cylinder, Phys. Fluids **25**, 013601 (2013).

[24] P. T. Tokumaru and P. E. Dimotakis, Rotary oscillation control of a cylinder wake, J. Fluid Mech. **224**, 77 (1991).

[25] A. Placzek, J.-F. Sigrist, and A. Hamdouni, Numerical simulation of an oscillating cylinder in a cross-flow at low Reynolds number: Forced and free oscillations, Comput. Fluids **38**, 80 (2009).

[26] Y. Tanida, A. Okajima, and Y. Watanabe, Stability of a circular cylinder oscillating in uniform flow or in a wake, J. Fluid Mech. **61**, 769 (1973).

[27] Q. M. Al-Mdallal, K. P. Lawrence, and S. Kocabiyic, Forced streamwise oscillations of a circular cylinder: Locked-on modes and resulting fluid forces, J. Fluids Struct. **23**, 681 (2007).

[28] S. Baek and H. J. Sung, Numerical simulation of the flow behind a rotary oscillating circular cylinder, Phys. Fluids **10**, 869 (1998).

[29] B. J. Armstrong, F. H. Barnes, and I. Grant, A comparison of the structure of the wake behind a circular cylinder in a steady flow with that in a perturbed flow, Phys. Fluids **30**, 19 (1987).

[30] O. M. Griffin and M. S. Hall, Review—Vortex shedding lock-on and flow control in bluff body wakes, J. Fluids Eng. **113**, 526 (1991).

[31] S. Barbi, D. P. Favier, C. A. Maresca, and D. P. Telionis, Vortex shedding and lock-on of a circular cylinder in oscillatory flow, J. Fluid Mech. **170**, 527 (1986).

[32] J. R. Filler, P. L. Marston, and W. C. Mih, Response of the shear-layer separating from a circular cylinder to small-amplitude rotational oscillations, J. Fluid Mech. **231**, 481 (1991).

[33] See Supplemental Material at http://link.aps.org/supplemental/10.1103/PhysRevFluids.6.034401 for the simulated wake flow past the stationary cylinder; videos of the cylinder wakes synchronized to the rotary, cross-flow, and streamwise oscillations with the lowest mean drag; and an animation of the wake flow phase-locked to the superimposition of the rotary and cross-flow vibrations. The parameters of the last example are selected such that the synchronizability parameter S is minimized.

[34] J. Carberry, J. Sheridan, and D. Rockwell, Forces and wake modes of an oscillating cylinder, J. Fluids Struct. **15**, 523 (2001).